Towards Systematic Design of General Type-2 Fuzzy Logic Controllers: Analysis, Interpretation and Tuning

Ahmet Sakalli, *Graduate Student Member, IEEE*, Tufan Kumbasar, *Senior Member, IEEE,* and Jerry M. Mendel, *Life Fellow, IEEE*

***Abstract*—This paper aims to provide a new perspective on how the deployment of General Type-2 (GT2) fuzzy sets affects the mapping of a class of Fuzzy Logic Controllers (FLCs). It is shown that an α-plane represented GT2-FLC is easily designed via baseline type-1 and interval type-2 FLCs; and two Design Parameters (DPs). The DPs are the total number of α-planes and the tuning parameter of the secondary membership function which are interpreted as sensitivity and shape DPs, respectively. We provide a clear understanding and interpretation of the sensitivity and shape DPs on controller performance through various comparative analyses. We present design approaches on how to tune the shape DP by providing a tradeoff between robustness and performance. We also propose two online scheduling mechanisms to tune the shape DP. We explore the effect of the sensitivity DP on the GT2-FLC and provide practical insights on how to tune the sensitivity DP. We present an algorithm for tuning the sensitivity DP that provides a compromise between computational time and sensitivity. We validate our analyses, interpretations, and design methods with experimental results conducted on a drone. We believe that the paper provides clear explanations on the role of DPs on the performance, robustness, sensitivity, and computational time of GT2-FLCs.**

***Index Terms*— General type-2 fuzzy logic controllers, type-2 fuzzy sets, secondary membership function, systematic design**

I. Introduction

Fuzzy Logic Controllers (FLCs) have been widely designed and deployed for various control applications [1-30]. In the last two decades, the research has been predominantly focused on Interval Type-2 (IT2) FLCs, as they are able to achieve better control system performances than their T1 counterparts [6-19]. It is also shown that IT2-FLCs are potentially more robust than their T1 counterparts, as their Control Curves (CCs) / Control Surfaces (CSs) are usually smooth around the steady state [7, 10-12, 17]. These potential improvements of IT2-FLCs mainly occur due to the extra degree of freedom provided by the Footprint of Uncertainty (FOU) in their antecedent Membership Functions (MFs) that are defined by IT2 Fuzzy Sets (FSs). In our previous works [12, 17-20], we have shown that smooth or aggressive CCs/CSs can be easily generated by tuning the parameters that define the size of the FOU.

Recently, researchers have given more attention to General Type-2 (GT2) FLCs as it is shown that GT2-FLCs outperform their T1 and IT2 counterparts [1, 2, 22-30]. This is due to the fact that GT2-FLCs use and process GT2-FSs, i.e. employ T1-FSs as Secondary MFs (SMFs) instead of interval FSs [1, 2], and thus naturally have more parameters (i.e. design flexibility) to be tuned in comparison to their IT2 counterpart [22, 30]. Therefore, one might conclude that the structure and design of GT2-FLCs is more complex. Yet, via the zSlices [21] or α-plane [31] representations, the output of a GT2-FLC can be easily defined by aggregating a collection of T1 and IT2 FLCs [1].

Quite recently, the following research question was asked [28] "*Why does improved performance occur as one goes from crisp, to T1, to IT2, to GT2 fuzzy systems?"*. To seek an answer, Mendel [28] investigated the first-order and second-order rule partitions and novelty partitions of GT2-FLCs and provided new perspectives to find the underlying reasons for the potential performance improvements of GT2-FLCs comparing to their IT2, T1 and non-fuzzy counterparts. In [22], the effects of the SMFs (in terms of size and shape) on the control performance were investigated by employing zSlices representation. It was stated that designing GT2-FSs is relatively more complex than IT2-FSs due to the difficulty of tuning the Design Parameters (DPs) [22]. Yet, it has been shown that GT2-FLCs can provide an acceptable tradeoff between robustness and performance by tuning the SMFs.

In this paper, motivated by the research question in [28], we examine a class of GT2-FLCs and provide new insights into how the deployment of GT2-FSs affects the CC/CS generation, and we propose systematic design approaches to construct and tune GT2-FLCs. In this context, after presenting their T1 and IT2 counterparts, we handle and examine single and double input GT2-FLCs that are represented with α-planes.

We first suggest the use of SMFs with trapezoid T1-FSs because they include the widely used crisp, interval and triangular SMFs. Then, to facilitate the design of the SMFs, we propose a new parameterization method to define trapezoid SMFs based on a single tuning parameter.

A. Sakalli and T. Kumbasar are with the Control and Automation Engineering Department, Istanbul Technical University, 34469, Istanbul, Turkey (e-mail: sakallia@itu.edu.tr, kumbasart@itu.edu.tr).

J. M. Mendel is Professor Emeritus at University of Southern California, Los Angeles, CA 90089-2564, USA (e-mail: mendel@sipi.usc.edu), and Tianjin 1000-Talents Foreign Experts Plan Endowment Professor and Honorary Dean of the College of Artificial Intelligence, Tianjin Normal University, Tianjin, China.

This work was supported by the Research Fund of the Scientific and Technological Research Council of Turkey under Project 118E807.

We provide general suggestions on the structural setting of GT2-FLC not only to construct GT2-FLCs in a straightforward manner but also to reduce the total number of DPs. Then, we present the main DPs of the GT2-FLCs by providing them interpretations with respect to their effects on the sensitivity and shape of the resulting CC/CS. We suggest using the total number of α-planes as a sensitivity DP and the tuning parameter of the SMFs as a shape DP. To validate the interpretations of the DPs, we present comparative analyses.

We investigate the effect of the shape DP on the CC/CS and then provide explanations about the role of the shape DP on the potential improvements to performance and robustness. Based on comparative investigations, we present design recommendations on how to tune the shape DP by providing a tradeoff between robustness and performance. Moreover, we present two novel online Scheduling Mechanisms (SMs) that tune the shape DP with respect to the steady state Operating Points (OPs) and transient state dynamics.

We explore the effect of the sensitivity DP on the CC/CS and provide practical insights on how to tune the sensitivity DP. Through the presented comparative results, we suggest tuning the sensitivity DP by considering the resolutions and processing speed limitations of the hardware components, which are the quantization level and Computational Time (CT). In order to provide a compromise between sensitivity and CT, we propose an iterative algorithm to tune the sensitivity of DP.

We also present experimental results using the Parrot Mambo drone, which acts as a real-world platform, to evaluate the proposed design recommendations/methods for GT2-FLCs.

In Table I, the widely used abbreviations in this paper are given for the convenience of the reader.

TABLE I
ABBREVIATIONS AND THEIR DESCRIPTIONS

Abbreviation	Description
ACT	Average Computational Time
CC	Control Curve
CS	Control Surface
CT	Computational Time
DFLC	Double-Input Fuzzy Logic Controller
DP	Design Parameter
FLC	Fuzzy Logic Controller
FOU	Footprint of Uncertainty
FS	Fuzzy Set
GT2	General Type-2
IT2	Interval Type-2
LMF	Lower Membership Function
MF	Membership Function
OP	Operating Point
SFLC	Single-Input Fuzzy Logic Controller
SM	Scheduling Mechanism
SMF	Secondary Membership Function
T1	Type-1
UMF	Upper Membership Function
α-T2-FLC	IT2-FLC associated with an α-plane α_p

II. PRELIMINARIES ON T1 AND IT2 FLCs

The state-of-the-art fuzzy controllers are the PID type SFLC and DFLC [10-13, 15-17]. The PID type SFLC is composed of a FLC cascaded to a PID controller [12], while the DFLC one is composed of a PD type FLC with an integrator and a summation unit [13]. Brief information on the structure of PID type SFLCs and DFLCs is given in the Supplementary Material.

A. The Internal Structures of Single Input T1 and IT2 FLCs

A SFLC is constructed by selecting its input as the error ($x_1 = E$) and the output is denoted as y [12]. We prefer to construct SFLCs composed of $N = 3$ ($n = 1, 2, 3$) rules as shown in Table II. The rules of a SFLC employing T1-FSs (the bold lines in Fig. 1) $A_{j,i}$ ($j = 1$ and $i = 1, 2, 3$) are:

$$R_n\text{: IF } x_1 \text{ is } A_{1,i} \text{ THEN } y \text{ is } C_n \tag{1}$$

while the structure of the SFLCs employing IT2-FSs ($\tilde{A}_{j,i}$) (shown in Fig. 1) are:

$$R_n\text{: IF } x_1 \text{ is } \tilde{A}_{1,i} \text{ THEN } y \text{ is } C_n \tag{2}$$

where C_n is a crisp consequent MF; n, j, and i denote the indexes for rules, inputs, and antecedent MFs, respectively. Note that, as IT2-FSs are employed, $\mu_{\tilde{A}}(x,u) = 1$ holds for $\forall u \in J_x \subseteq [0,1]$ where J_x is the primary membership of $\tilde{A}_{j,i}$ [1].

The output of the T1-SFLC is defined as follows [1]:

$$y_{T1} = \frac{\sum_{n=1}^{N} f_n C_n}{\sum_{n=1}^{N} f_n} \tag{3}$$

Here f_n denotes firing strength and is defined as:

$$f_n = \mu_{A_{1,i}} \tag{4}$$

where $\mu_{A_{j,i}}$ is defined for an input x_j as follows:

$$\mu_{A_{j,i}} = \begin{cases} \dfrac{x_j - c_{j,i-1}}{c_{j,i} - c_{j,i-1}}, & x_j \in [c_{j,i-1}, c_{j,i}] \\ \dfrac{c_{j,i+1} - x_j}{c_{j,i+1} - c_{j,i}}, & x_j \in [c_{j,i}, c_{j,i+1}] \end{cases} \tag{5}$$

Here $c_{j,i}$ is set as $c_{j,1} = -1$, $c_{j,2} = 0$, and $c_{j,3} = 1$ for $\forall j$.

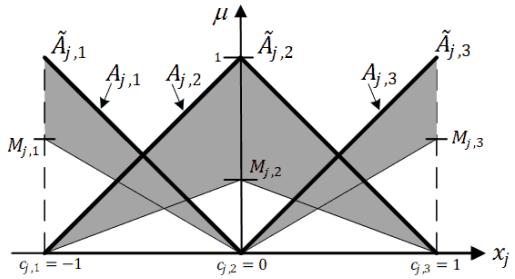

Fig. 1. Illustration of antecedent MFs of the T1 and IT2 FLCs

TABLE II
THE RULE BASE OF T1, IT2, AND GT2 SFLCS

x_1	[a] $A_{1,1}$ or [b] $\tilde{A}_{1,1}$	[a] $A_{1,2}$ or [b] $\tilde{A}_{1,2}$	[a] $A_{1,3}$ or [b] $\tilde{A}_{1,3}$
	$C_1 = -1$	$C_2 = 0$	$C_3 = 1$

[a] Defined for T1 SFLCs. [b] Defined for IT2 and GT2 SFLCs.

The output of the IT2-SFLC is defined as [1]:

$$y_{IT2} = \left(\underline{y}_{IT2} + \overline{y}_{IT2}\right)/2 \tag{6}$$

where $\underline{y}_{IT2}$ and $\overline{y}_{IT2}$ are defined as follows:

$$\underline{y}_{IT2} = \frac{\sum_{n=1}^{L} \overline{f_n} C_n + \sum_{n=L+1}^{N} \underline{f_n} C_n}{\sum_{n=1}^{L} \overline{f_n} + \sum_{n=L+1}^{N} \underline{f_n}} \tag{7}$$

$$\overline{y}_{IT2} = \frac{\sum_{n=1}^{R} \underline{f_n} C_n + \sum_{n=R+1}^{N} \overline{f_n} C_n}{\sum_{n=1}^{R} \underline{f_n} + \sum_{n=R+1}^{N} \overline{f_n}} \tag{8}$$

Here L, R are found via the Karnik-Mendel algorithm [1], $\overline{f_n}$ and $\underline{f_n}$ are upper and lower firing strengths that are defined as:

$$\left[\overline{f_n} \quad \underline{f_n}\right] = \left[\overline{\mu}_{\tilde{A}_{1,i}} \quad \underline{\mu}_{\tilde{A}_{1,i}}\right] \tag{9}$$

where $\overline{\mu}_{\tilde{A}_{j,i}}$ is the UMF defined as in (4), while $\underline{\mu}_{\tilde{A}_{j,i}}$ is the LMF is defined as follows:

$$\overline{\mu}_{\tilde{A}_{j,i}} = \mu_{A_{j,i}} \quad \underline{\mu}_{\tilde{A}_{j,i}} = \overline{\mu}_{\tilde{A}_{j,i}} M_{j,i} \tag{10}$$

where $M_{j,i}$ are the heights of the LMFs which are the main DPs of IT2-SFLCs [11, 12].

B. The Internal Structures of Double Input T1 and IT2 FLCs

The DFLC is constructed by selecting its inputs as the error and the change of error ($x = [E, \Delta E]$) that are partitioned with $I = 3$ ($i = 1, 2, 3$) and $K = 3$ ($k = 1, 2, 3$) MFs, respectively [11]. Thus, we define $N = 3x3$ ($n = 1,2, \ldots, 9$) rules as in Table III. The rule structure of a DFLC employing T1-FSs is as:

$$R_n\text{: IF } x_1 \text{ is } A_{1,i} \text{ AND } x_2 \text{ is } A_{2,k} \text{THEN } y \text{ is } C_n \tag{11}$$

while the rule structure of a DFLC employing IT2-FSs is as:

$$R_n\text{: IF } x_1 \text{ is } \tilde{A}_{1,i} \text{ AND } x_2 \text{ is } \tilde{A}_{2,k} \text{ THEN } y \text{ is } C_n \tag{12}$$

The output of the T1-DFLC is calculated as in (3), with respect to Table III, in which the firing strengths are defined as:

$$f_n = \mu_{A_{1,i}} \times \mu_{A_{2,k}} \tag{13}$$

where $\times$ indicates the product t-norm operator.

The output of the IT2-DFLC is calculated as in (6) with $\overline{f_n}$ and $\underline{f_n}$ that are defined as follows:

$$\overline{f_n} = \overline{\mu}_{\tilde{A}_{1,i}} \times \overline{\mu}_{\tilde{A}_{2,k}} \quad \underline{f_n} = \overline{\mu}_{\tilde{A}_{1,i}} M_{1,i} \times \overline{\mu}_{\tilde{A}_{2,k}} M_{2,k} \tag{14}$$

Here $\overline{\mu}_{\tilde{A}_{1,i}}$ and $\overline{\mu}_{\tilde{A}_{2,k}}$ are calculated as given in (10). $M_{1,i}$ and $M_{2,k}$ are the heights of the LMFs defined for the inputs x_1 and x_2, respectively. Similar to its SFLC counterpart, $M_{1,i}$ and $M_{2,k}$ are the main DPs of IT2-DFLCs [16-20].

TABLE III
THE RULE BASE OF T1, IT2, AND GT2 DFLCS

$x_2 \setminus x_1$	[a] $A_{1,1}$ or [b] $\tilde{A}_{1,1}$	[a] $A_{1,2}$ or [b] $\tilde{A}_{1,2}$	[a] $A_{1,3}$ or [b] $\tilde{A}_{1,3}$
[a] $A_{2,1}$ or [b] $\tilde{A}_{2,1}$	$C_1 = -1$	$C_2 = -0.8$	$C_3 = 0$
[a] $A_{2,2}$ or [b] $\tilde{A}_{2,2}$	$C_4 = -0.8$	$C_5 = 0$	$C_6 = 0.8$
[a] $A_{2,3}$ or [b] $\tilde{A}_{2,3}$	$C_7 = 0$	$C_8 = 0.8$	$C_9 = 1$

[a] Defined for T1-DFLCs. [b] Defined for IT2 and GT2 DFLCs.

III. GT2-FLCS: STRUCTURAL DESIGN RECOMMENDATIONS

We first present the internal structures of GT2 counterparts of the given FLCs. We propose a parameterization to simplify the design of SMFs and then provide recommendations on how to interpret the DPs of GT2-FLCs.

A. Single-Input and Double-Input GT2-FLCs

The rule structures of the GT2 SFLCs and DFLCs are constructed over their baseline T1 and IT2 FLCs. Therefore, our GT2-FLCs have the same rule base (as given in (2) and (12)) and the same MFs at the primary level as their IT2 fuzzy counterparts. The fundamental difference between an IT2-FLC and a GT2-FLC is that the GT2-FLCs use and process T1-FSs as SMFs instead of an interval set ($\mu_{\tilde{A}}(x,u) = 1$ for $\forall u \in J_x \subseteq [0,1]$). It is known that the GT2-FSs, employed in the antecedent part of the rules, can be defined as a collection of α-planes (α_p) as follows [1, 32]:

$$\tilde{A}_{j,i} = \bigcup_{\alpha_p \in [0,1]} \tilde{A}_{j,i}^{\alpha_p} \tag{15}$$

where $\tilde{A}_{j,i}^{\alpha_p}$ is an α-plane of $\tilde{A}_{j,i}$ associated with α_p (i.e, an α-plane raised to level α_p or a zSlice [1]). Hence, the output of the GT2-FLC can be defined as [1, 33]:

$$y_{GT2} = \left(\sum_{p=1}^{P} y_{GT2}^{\alpha_p}\, \alpha_p\right) \Big/ \left(\sum_{p=1}^{P} \alpha_p\right) \tag{16}$$

where $y_{GT2}^{\alpha_p}$ is the output of IT2-FLC (or T1-FLC) associated with an α-plane α_p (α-T2-FLC), and P ($p = 1, \ldots P$) is the total number of α-planes (excluding $\alpha_0 = 0$). This representation gives opportunity to define the output of GT2-FLC (y_{GT2}) as an aggregation of α-plane outputs ($y_{GT2}^{\alpha_p}$), which are principally the outputs of T1-FLC (y_{T1}) and IT2-FLCs (y_{IT2}) [1, 22].

B. A Novel Representation of Trapezoid SMFs

Let us define the SMF of the GT2-FS with trapezoid T1-FSs as shown in Fig. 2. The corresponding UMF and LMF of an α-T2-FLC are then defined as follows:

$$\underline{\mu}_{\tilde{A}_{j,i}^{\alpha_p}} = \underline{\mu}_{\tilde{A}_{j,i}} + \left(\overline{\mu}_{\tilde{A}_{j,i}} - \underline{\mu}_{\tilde{A}_{j,i}}\right)\left(\delta_{j,i}^{1} + \alpha_p\left(\delta_{j,i}^{2} - \delta_{j,i}^{1}\right)\right) \tag{17}$$

$$\overline{\mu}_{\tilde{A}_{j,i}^{\alpha_p}} = \overline{\mu}_{\tilde{A}_{j,i}} - \left(\overline{\mu}_{\tilde{A}_{j,i}} - \underline{\mu}_{\tilde{A}_{j,i}}\right)\left(1 - \delta_{j,i}^{4} + \alpha_p\left(\delta_{j,i}^{4} - \delta_{j,i}^{3}\right)\right) \tag{18}$$

where $\delta_{j,i}^{t}$ ($t = 1, 2, 3, 4$) defines the shape and size of the SMF. Note that, $0 \le \delta_{j,i}^{1} \le \delta_{j,i}^{2} \le \delta_{j,i}^{3} \le \delta_{j,i}^{4} \le 1$.

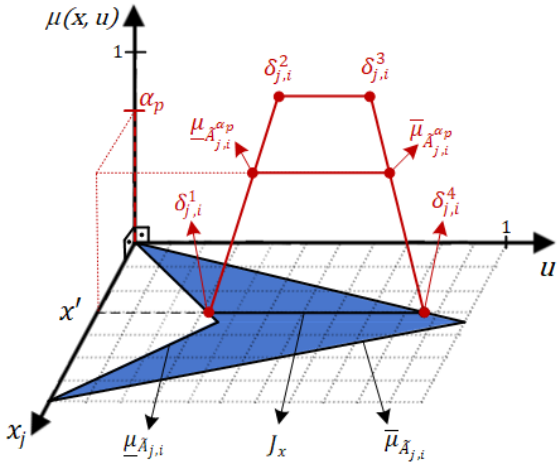

Fig. 2. Illustration of a GT2-FS with α-plane

In the design of GT2-FLCs, we suggest the use of trapezoid SMFs, since it is possible to obtain various SMFs with different shapes and supports with respect to $\delta_{j,i}^{t}$.

The support of the SMF is defined on the primary MF J_x, if

$$\delta_{j,i}^{1} = 0, \quad \delta_{j,i}^{1} \le \delta_{j,i}^{2} \le \delta_{j,i}^{3} \le \delta_{j,i}^{4}, \quad \delta_{j,i}^{4} = 1 \tag{19}$$

is satisfied, whereas for

$$\delta_{j,i}^{1} > 0, \quad \delta_{j,i}^{1} \le \delta_{j,i}^{2} \le \delta_{j,i}^{3} \le \delta_{j,i}^{4}, \quad \delta_{j,i}^{4} < 1 \tag{20}$$

the support is defined on a subset of J_x which can be interpreted as resizing the FOU of the primary MF.

The shape of SMF can be also transformed via $\delta_{j,i}^{t}$. The following SMFs can be obtained:

- An interval SMF, if

$$\delta_{j,i}^1 = \delta_{j,i}^2 = 0, \quad \delta_{j,i}^3 = \delta_{j,i}^4 = 1 \tag{21}$$

and thus, the GT2-FSs $(\tilde{A}_{j,i})$ transform into IT2-FS.

- A crisp SMF, if

$$\delta_{j,i}^t = 1 \text{ or } \delta_{j,i}^t = 0\,, \forall t \tag{22}$$

and this reduces the antecedent GT2-FSs into T1-FSs.

- A triangle SMF for

$$\delta_{j,i}^1 \geq 0, \quad \delta_{j,i}^1 \leq \delta_{j,i}^2 = \delta_{j,i}^3 \leq \delta_{j,i}^4, \quad \delta_{j,i}^4 \leq 1 \tag{23}$$

Although trapezoid T1-FSs provide more design flexibility in defining the shape and support of the SMFs, the design is relatively complex as there are 4 parameters to be tuned.

In this study, in order to reduce the design complexity of the trapezoid SMF, we propose a simple parameter mapping that defines parameters ($\delta_{j,i}^t \in [0,1]$) with a single parameter as:

$$\begin{aligned} \delta_{j,i}^1 &= \min\left(\max\left(\theta_{j,i} - 1, 0\right), 1\right) \\ \delta_{j,i}^2 &= \min\left(\max\left(\theta_{j,i}, 0\right), 1\right) \\ \delta_{j,i}^3 &= \min\left(\max\left(\theta_{j,i} + 1, 0\right), 1\right) \\ \delta_{j,i}^4 &= \min\left(\max\left(\theta_{j,i} + 2, 0\right), 1\right) \end{aligned} \tag{24}$$

where $\theta_{j,i} \in [-2, 2]$ is the new DP of the SMF. The effect of DP on the shape and support of SMF is shown in Fig. 3 for $\theta_{j,i} \in [-2, 2]$. It can be seen that it is possible to generate various SMFs with this mapping. For example, the SMF parameters for $\theta_{j,i} = -0.5$ are calculated via (24) as $\delta_{j,i}^1 = 0$, $\delta_{j,i}^2 = 0$, $\delta_{j,i}^3 = 0.5$, and $\delta_{j,i}^4 = 1$ and the SMF shown in Fig. 3b is generated.

C. *Comments and Suggestions*

Here, we provide general suggestions on the structural setting of GT2-FLC and then present the main DPs of GT2-FLC.

We firstly suggest constructing the GT2-FLC by designing baseline T1 and IT2 FLCs as presented in Section II. This setting gives the opportunity to calculate the membership grades of each α-T2-FLC as given in (17) and (18) via the ones of the baseline T1 and IT2 FLCs. Then, the corresponding firing intervals of each α-T2-FLC are calculated to obtain the outputs $y_{GT2}^{\alpha_p}$ which are then aggregated via (16) to calculate the crisp output y_{GT2}. Thus, in the design of GT2-FLCs, we assume that the baseline tuning parameters (primary MFs of antecedent IT2-FSs and consequent MFs) and structural settings (rule base, aggregation/union operators, type-reduction) are set and fixed. Consequently, we only focus on the DPs provided by SMFs.

The main DPs of GT2-FLCs are the a-plane values (α_p), the total number of α-planes (P) and the tuning parameters of the SMF. We suggest handling these DPs as follows:

- It can be observed from (16) that the weighted average calculation can be seen as a quantization of a continuous integration. If α_p is evenly distributed, then we can define:

$$\alpha_p = p/P, \qquad p = 1, \dots, P \tag{25}$$

Thus, as P increases, the input-output mapping becomes closer to its continuous counterpart in terms of sensitivity/ accuracy. Therefore, *we suggest handling the total number of α planes (P) as the sensitivity DP of the GT2-FLCs*.

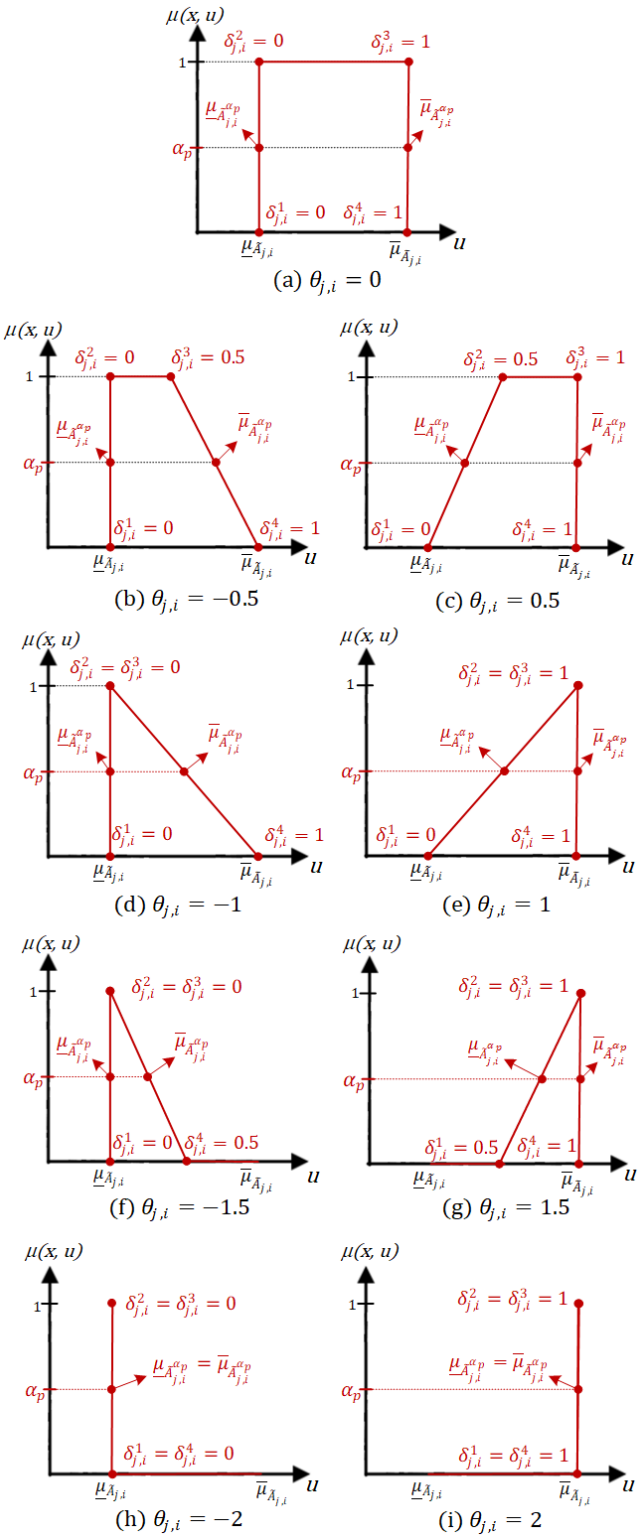

Fig. 3. Illustration of the trapezoid SMF for $\theta_{j,i} \in [-2, 2]$.

- It can be seen from (17-23) that the membership degrees of α-T2-FLCs are defined with respect to the shape of the SMFs which directly influences the resulting value of $y_{GT2}^{\alpha_p}$. Therefore, *we suggest handling the parameters that define the shape of the SMF as the shape DPs of the GT2-FLCs*.

In Table IV, DPs and #DP of GT2-FLCs are tabulated for each possible design configuration. We suggest to

- Use SMFs as defined in (24) since this parameterization reduces not only the #DP significantly but also provides the opportunity to the designer to construct various shapes of SMFs with a single design parameter as shown in Fig. 3.
- Define the same SMF for each antecedent GT2-FS to decrease the design complexity/effort. This structural setting reduces #DP since the design is accomplished with a single shape DP, denoted as θ ($\theta_{j,i} = \theta\ \forall i,j$).

In summary, we suggest constructing the GT2-FLCs that are highlighted with bold in Table IV.

In the design of GT2-FLC, we first suggest to tune the shape DP (θ) to end up with desired controller performance measures and then to tune the sensitivity DP (P) with respect to the sensitivity/accuracy measures. We present analyses to provide design methods/recommendations to tune the shape and sensitivity DPs in Sections IV and V, respectively.

TABLE IV
DESIGN PARAMETERS OF GT2-FLC

	#Inputs	Property*	DP*	#DP
1	Single	Unique SMF for $\tilde{A}_{1,i}$	$\delta^t_{1,i}$, P	13
2	Single	Same SMF for $\forall\tilde{A}_{1,i}$	δ^t, P	5
3	Single	Unique SMF for $\tilde{A}_{1,i}$	$\theta_{1,i}$, P	4
4	**Single**	**Same SMF for $\forall\tilde{A}_{1,i}$**	$\boldsymbol{\theta}$**,** $\boldsymbol{P}$	**2**
5	Double	Unique SMF for $\tilde{A}_{j,i}$	$\delta^t_{j,i}$, P	25
6	Double	Same SMF for $\forall\tilde{A}_{j,i}$	δ^t, P	5
7	Double	Unique SMF for $\tilde{A}_{j,i}$	$\theta_{j,i}$, P	7
8	**Double**	**Same SMF for $\forall\tilde{A}_{j,i}$**	$\boldsymbol{\theta}$**,** $\boldsymbol{P}$	**2**

* $j = (1,2)$, $i = (1,2,3)$, $t = (1,2,3,4)$, $\delta^t = \delta^t_{j,i}\ \forall i,j,t$

IV. THE SHAPE DESIGN PARAMETER OF GT2-FLCS: ANALYSES AND DESIGN

In this section, we first investigate the effect of the shape DP (θ) on the GT2 CC/CS generation, and then present design recommendations and online SMs to tune the shape DP.

Let us firstly examine how the structure of the GT2-FLC changes with respect to $\theta \in [-2,2]$. It can be observed from:

- Fig. 3a that $\underline{\mu}_{\tilde{A}^{\alpha_p}_{j,i}} = \underline{\mu}_{\tilde{A}^{\alpha_0}_{j,i}}$ and $\overline{\mu}_{\tilde{A}^{\alpha_p}_{j,i}} = \overline{\mu}_{\tilde{A}^{\alpha_0}_{j,i}}, \forall\alpha_p$ for $\theta = 0$. Thus, as an interval SMF is obtained, the GT2-FLC reduces to the baseline IT2-FLC given in Section II.
$$y_{GT2}\Big|_{\theta=0} = y_{IT2} \tag{26}$$
The GT2-FLC results with the same CC/CS of its IT2 baseline counterpart.
- Fig. 3h that $\underline{\mu}_{\tilde{A}^{\alpha_p}_{j,i}} = \overline{\mu}_{\tilde{A}^{\alpha_p}_{j,i}} = \underline{\mu}_{\tilde{A}^{\alpha_0}_{j,i}}, \forall\alpha_p$ for $\theta = -2$. In this case, the GT2-FLC reduce to a T1-FLC, that only uses the LMFs of the IT2-FSs, which is defined as:
$$y_{GT2}\Big|_{\theta=-2} = \frac{\sum_{n=1}^{N} \underline{f_n} C_n}{\sum_{n=1}^{N} \underline{f_n}} \tag{27}$$
- Fig. 3i that $\underline{\mu}_{\tilde{A}^{\alpha_p}_{j,i}} = \overline{\mu}_{\tilde{A}^{\alpha_p}_{j,i}} = \overline{\mu}_{\tilde{A}^{\alpha_0}_{j,i}}\ \forall\alpha_p$ for $\theta = 2$. Thus, as the SMF reduces to a crisp value, the GT2-FLC reduces to a T1-FLC, that only uses the UMFs of the IT2-FSs, that is
$$y_{GT2}\Big|_{\theta=2} = y_{T1} \tag{28}$$
which is its baseline T1-FLC defined in Section II. Thus, the GT2-FLC results with the CC/CS of its T1 counterpart.

It can be concluded that by simply varying θ various T1 and IT2 FLCs can be obtained. Also, as $\theta \in \{-2,0,2\}$ are the structure switching values, the output of the GT2-FLC is over bounded as follows:
$$\underline{y}_{GT2} \le y_{GT2} \le \overline{y}_{GT2} \tag{29}$$
where
$$\underline{y}_{GT2} = \min_{\theta\in\{-2,0,2\}} y_{GT2}\Big|_{\theta},\quad \overline{y}_{GT2} = \max_{\theta\in\{-2,0,2\}} y_{GT2}\Big|_{\theta} \tag{30}$$

A. Shape Analyses of the Control Curves / Control Surfaces

Here, we analyze the CCs/CSs of GT2-FLCs employing P=10 α-planes for $\theta \in$ {-2, -1.5,-1, -0.5, 0, 0.5, 1, 1.5, 2} that result with the SMFs depicted in Fig. 3. As is suggested to construct the GT2-FLC with baseline T1 and IT2 FLCs in Section III, we define the IT2-SFLCs with two different FOU DP ($M_{j,i}$) settings as follows:

- IT2-SFLC which has a smooth CC:
  FOU-1: $M_{1,1} = 0.2$, $M_{1,2} = 0.9$, $M_{1,3} = 0.2$.
- IT2-SFLC which has an aggressive CC:
  FOU-2: $M_{1,1} = 0.9$, $M_{1,2} = 0.2$, $M_{1,3} = 0.9$.

These FOU DPs are set according to the design method given in [12]. The baseline T1-SFLC is given in Section II. For the GT2-DFLCs, we define the following baselines:

- IT2-DFLC which has a smooth CC around the origin:
  FOU-3: $M_{1,1} = 0.2$, $M_{1,2} = 0.9$, $M_{1,3} = 0.2$, $M_{2,1} = 0.2$, $M_{2,2} = 0.9$, and $M_{2,3} = 0.2$.
- IT2-DFLC which has an aggressive CC around the origin:
  FOU-4: $M_{1,1} = 0.9$, $M_{1,2} = 0.3$, $M_{1,3} = 0.9$, $M_{2,1} = 0.9$, $M_{2,2} = 0.3$, and $M_{2,3} = 0.9$.

The IT2-DFLCs are tuned via the design suggestions given in [18-20] while the T1-DFLC is as given in Section II.

Now, in order to clearly show the effect of shape DP (θ) on the CC/CS, we define two measures to analyze the resulting impact. The first measure is the Normalized Total Energy (NTE) of the CC/CS which is defined as follows:
$$NTE = \|y_{GT2}\|_2 / \|y_{T1}\|_2 \tag{31}$$
The NTE measure provides us information on the smoothness/ aggressiveness of the CC/CS of the GT2-FLC with respect to its T1 counterpart. For instance, if $NTE > 1$, then the CC/CS of the GT2-FLC is relatively more aggressive as it has more energy than its T1 counterpart. Moreover, to examine the robustness of FLCs around the steady state, we define a zero-mean gaussian noise with a standard deviation of $\sigma_{in} = 0.2$ as an input and calculate the following ratio:
$$NR = \sigma^2_{out} / \sigma^2_{in} \tag{32}$$
where σ_{out} is the standard deviation of the GT2-FLC output. For instance, if $NR < 1$, then the handled FLC is potentially more robust against noises and uncertainties.

1) Shape Analyses for GT2-SFLCs

The resulting CC of GT2-SFLC with FOU-1 is illustrated in Fig. 4, while the one with FOU-2 is given in the Supplementary Material. Here, we only analyzed the CCs for $x_1 \in [0,1]$ since CCs are symmetric with respect to $x_1 = 0$ [12]. It can be concluded that the DP θ, which defines the shape of the SMF, shapes the resulting CC.

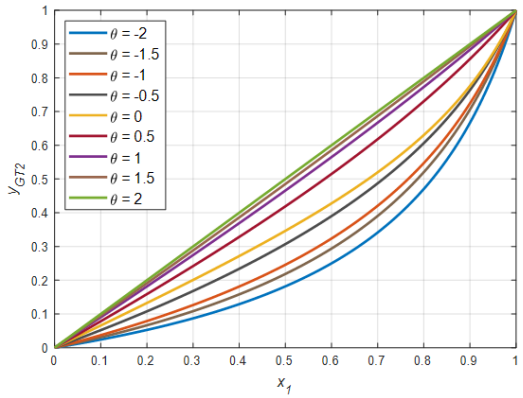

Fig. 4. Effect of the shape DP θ on CCs of GT2-FLCs with FOU-1

It can be observed that, as θ decreases from 2 to -2, the resulting CC becomes smoother for FOU-1, while more aggressive for FOU-2. This also coincides with the measures given in Table V. The highest NTE value is obtained for the GT2-SFLC with the setting of FOU-2 and $\theta = -2$. Therefore, the resulting controller has an aggressive CC and thus a potential to improve system response. Moreover, the lowest NR is obtained for the GT2-SFLC with FOU-1 and $\theta = -2$. Thus, a potentially more robust controller can be obtained as it is less sensitive to noise around the origin in comparison to its GT2 counterparts.

TABLE V
PERFORMANCE MEASURES FOR GT2-FLCS

	GT2-SFLC				GT2-DFLC			
	FOU-1		FOU-2		FOU-3		FOU-4	
θ	NTE	NR	NTE	NR	NTE	NR	NTE	NR
-2	0.633	0.093	1.341	5.272	0.736	0.344	1.143	6.638
-1.5	0.679	0.141	1.297	4.420	0.770	0.485	1.125	5.970
-1	0.707	0.189	1.266	3.978	0.787	0.609	1.106	5.502
-0.5	0.772	0.324	1.199	3.091	0.829	0.948	1.065	4.542
0	0.805	0.455	1.156	2.733	0.846	1.230	1.028	4.063
0.5	0.910	0.658	1.079	1.627	0.935	1.743	1.025	3.308
1	0.963	0.841	1.033	1.230	0.974	2.154	1.012	2.818
1.5	0.985	0.925	1.015	1.088	0.990	2.337	1.007	2.633
2	1.000	1.000	1.000	1.000	1.000	2.491	1.000	2.491

2) Shape Analyses for GT2-DFLCs

The resulting CS of GT2-DFLC with FOU-3 is given in Fig. 5, while the one with FOU-4 is presented in the Supplementary Material. However, analyzing the shape of CSs is not straightforward as the CCs. Thus, we analyzed also the differences between the CSs ($y_{GT2} - y_{T1}$ and $y_{GT2} - y_{IT2}$) for both FOU-3 and FOU-4 settings by varying the shape DP (given in the Supplementary Material). It can be seen from the presented results that shape DP θ has a similar effect on the CS generation as in its single input counterpart. This can be also clearly seen from the calculated measures given in Table V. For instance, for the FOU-3 setting, the robustness of the system increases while the θ value changes from 2 to -2. Here, the lowest NTE and NR values are obtained for the GT2-DFLC with FOU-3 and $\theta = -2$. Thus, it has a potential to achieve more robust performance, as it is more capable to mitigate the noise than its counterparts. On the other hand, decreasing the value of θ from 2 to -2, increases the aggressiveness of the GT2-DFLC with FOU-4 (constructed with an aggressive baseline IT2-DFLC) since the NTE value increased by almost 15%. However, the robustness level of resulting GT2-DFLC reduces against noise, as the NR value increased.

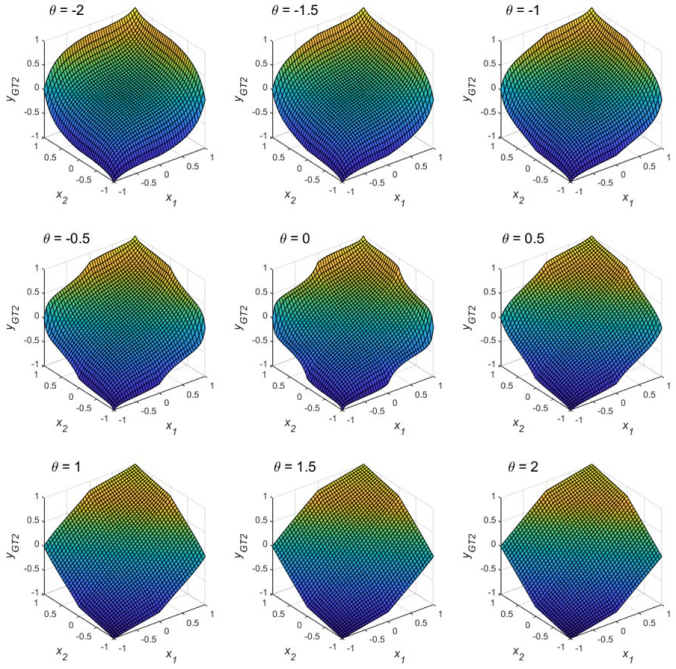

Fig. 5. Effect of the shape DP θ on CSs of GT2-FLCs with FOU-3

B. Comments and Suggestions on the Shape DP

It can be concluded that the shape DP (θ) defines the resulting CC/CS of the GT2-FLC. Thus, tuning the shape of the SMF might be an efficient way to design GT2-FLCs as the properties of the baseline FLCs can be preserved. On the other hand, the impact of θ on the shape of CC/CS (smooth or aggressive) depends on the baseline T1 and IT2 FLCs.

In the design of the GT2-FLC, we suggest designing the T1-FLC, i.e. $y_{GT2}|_{\theta=2}$, and IT2-FLC, i.e. $y_{GT2}|_{\theta=0}$, baselines, with aggressive and smooth CCs/CSs, respectively (as it is usually done in the fuzzy control literature [6, 10, 12]). Thus, $|y_{IT2}| \leq |y_{T1}|\ \forall x$ (or almost all) satisfies, and then (29) becomes

$$\left|y_{GT2}\right|_{\theta=-2}\left| \leq |y_{GT2}| \leq \right|y_{GT2}\left|_{\theta=2}\right| \tag{33}$$

which can be also seen from Fig. 4. For this suggested baseline setting, we can comment that:

i) Decreasing θ from 2 to 0, converts the CC/CS of GT2-FLC from its baseline T1-FLC to its IT2-FLC counterpart as expected. Thus, the control performance and robustness of GT2-FLC with a $\theta \in [0,2]$ will always lie between the baseline T1-FLC and IT2-FLC.

ii) Decreasing θ from 0 to -2, the CC/CS of GT2-FLC transforms from its baseline IT2-FLC counterpart to a T1-FLC that only uses the LMFs as given in (27). Thus, designing a GT2-FLC with a $\theta \in [-2,0)$ gives the opportunity to design GT2-FLCs that are relatively more robust than its baseline IT2-FLC since (33) is satisfied.

It is worth to emphasize that the shape DP $\theta \in [-2, 2]$ provides not only a design simplicity as only baseline T1 and IT2 FLCs are needed, but also a convenient design flexibility, since various CCs/CSs can be generated straightforwardly by simply tuning a single parameter θ. We suggest designing the CC/CS of the GT2-FLC by employing the tuning steps summarized in Table VI.

TABLE VI
TUNING STEPS OF THE SHAPE DP

Step-1	Design a T1-FLC such that the system response is fast and satisfactory (i.e. aggressive CC/CS).
Step-2	Convert the T1-FLC to an IT2-FLC by tuning the FOU DPs to end up with a potentially robust controller (i.e. smooth CC/CS). Use the design guidelines/suggestions given in [12, 18-20].
Step-3	Use the designed T1- and IT2- FLCs as baselines to construct a GT2-FLC. Tune the shape DP θ (online or offline) by providing a tradeoff between robustness (i.e. like IT2-FLC) and control system performance (i.e. like T1-FLC).

Remark-1: In the literature, IT2-FLCs are usually designed with smooth CCs/CSs for handling uncertainties and noises [6, 7, 10, 12]. Thus, we do not suggest design guidelines for the case where an aggressive IT2-FLC is designed in comparison to its T1 counterpart (i.e. $|y_{IT2}| \geq |y_{T1}| \; \forall x$ (or almost all)). Though, similar/parallel observations can be also made for the structure when the baseline IT2-FLC is aggressive which is left for the reader. Note that, for this setting, (29) transforms to:

$$\left|y_{GT2}\right|_{\theta=2}\left| \leq |y_{GT2}| \leq \right|y_{GT2}\left|_{\theta=-2}\right| \tag{34}$$

This can be observed from figures in the Supplementary Material.

C. Online Scheduling Mechanisms for the Shape DP

The resulting control system performance improvements (in transient and steady states) of the GT2-FLCs for a θ value heavily depend on the OP in which the system is controlled, especially for nonlinear systems. Thus, the control system performance might be optimal/satisfactory at certain OP where the GT2-FLC is tuned, yet its performance might degrade at other OPs. This is due to the fact that the dynamics of nonlinear systems might change with respect to OPs. In control theory, this problem is usually solved with gain-scheduled controllers that use and schedule a collection of controllers, which are designed at various OPs, with respect to the steady state OP [4, 34]. Therefore, instead of tuning the shape DP (θ) in an offline manner, we suggest tuning the shape DP with an online SM by providing a tradeoff between the performance and robustness.

In this paper, we firstly propose the following SM to tune the shape DP with respect to steady state OPs:

SM-1: $$\theta_r = f_r(r) \tag{35}$$

where $f_r(r)$ is a mapping that calculates the value of $\theta = \theta_r$ with respect to the reference signal (r). The design steps of the SM-1 are accomplished as given in Table VII.

On the other hand, although tuning the shape DP via (35) is a simple way, the scheduling might not result in an efficient transient state control performance as only the steady state OPs are taken into account. So, we also recommend taking account the transient dynamics that occur during reference variation. In this context, we suggest one to use the following SM:

SM-2: $$\theta = \theta_r + w\,\theta_t \tag{36}$$

where w is a weighting coefficient and θ_t is varying parameter during the transient state to enhance the performance of GT2-FLC while approaching the steady state OP. The following design guidelines are proposed for shaping the value of θ_t:

- If the transient state response is fast, in order to prevent overshoot, the control signal should be smoothened. Hence, we suggest to set $\theta_t < 0$ to decrease the value of θ. With this setting, the CC/CS of GT2-FLC bends towards its boundary T1-FLC defined in (27).
- If the transient state response is slow then, to increase the convergence speed, the aggressiveness of the control signal should be increased. Therefore, we suggest to set $\theta_t > 0$ to increase the value of θ, i.e. the CC/CS of GT2-FLC bends towards its boundary T1-FLC defined in (28).
- At the steady state, we suggest $\theta_t = 0$ in order to set θ to its nominal value θ_r at the steady state OP (r).

TABLE VII
DESIGN STEPS OF THE ONLINE SM-1

Step-1	Define the OPs of the nonlinear system as $[r_1, r_2, \dots r_k]$.
Step-2	For each r_k, define a value of $\theta_r = \theta_{r_k}$. To accomplish such a goal, an optimization-based design can be performed.
Step-3	Define an interpolation method (i.e. linear, cubic, polynomial, fuzzy, etc.) for $f_r(r)$.

As the presented SM guidelines can be transformed to fuzzy rules, we propose a fuzzy SM $f_t(x)$ that generates θ_t as follows:

$$\theta_t = f_t(x) \tag{37}$$

where the input is defined as $x = [E, \Delta E]$ to capture the transient state dynamics of the control system as it has been widely done in the self-tuning FLCs [16, 18, 22]. The fuzzy SM is defined with the same antecedent T1-FSs and rule structure of the T1-DFLC presented in Section II. In the light of the SM design guidelines, we suggest the rule base in Table VIII to enhance the performance of the GT2-FLC. As it can be seen, the rules are symmetric on the left diagonal axis $x_1 = x_2$ so that a symmetric CS is obtained. We preferred to employ "0" and "-1" consequent values dominantly thus to prevent possible overshoots and oscillations. Also, in Table VIII, only the rule R_5 is activated at the steady state $(x_1 = x_2 = 0)$, and thus the output value becomes $\theta_t = 0$, and $\theta = \theta_r$. It is worth to mention that the consequent parameters are DPs and thus they should be tuned according to the control system dynamics. Yet, it has been observed that the ones given in Table VIII resulted in a satisfactory enhancement of the transient state.

TABLE VIII
THE RULE TABLE OF FUZZY SM $\boldsymbol{f_t(x)}$

$x_2 \;\backslash\; x_1$	$A_{1,1}$	$A_{1,2}$	$A_{1,3}$
$A_{2,1}$	$C_1 = 1$	$C_2 = 0$	$C_3 = -1$
$A_{2,2}$	$C_3 = 0$	$C_5 = 0$	$C_6 = -1$
$A_{2,3}$	$C_7 = -1$	$C_8 = -1$	$C_9 = -1$

V. THE SENSITIVITY DESIGN PARAMETER OF GT2-FLCS: ANALYSES AND DESIGN

In this section, the effect of the sensitivity DP (P) on the CC/CS is first examined to provide practical insight on how to tune P, after which a simple algorithm is proposed for tuning P.

A. Sensitivity Analyses of the Control Curves/Surfaces

We present comparative results in order to provide an insight into how the sensitivity DP affects the resulting CC/CS and the resulting CT. We analyze and compare GT2-FLCs employing $P = \{2, 3, 5, 10, 25, 100\}$ α-planes, with respect to both the Maximum Value of Errors (MVE) and the Mean Absolute Error (MAE) measures:

$$MVE(e_a^b) = \max_{v=1,\dots,V}(|e_a^b[v]|) \quad (38)$$

$$MAE(e_a^b) = \sum_{v=1}^{V} |e_a^b[v]|/V \quad (39)$$

where:

$$e_a^b[v] = Y_a[v] - Y_b[v] \quad (40)$$

V is the total number of samples, $Y_a[v]$ and $Y_b[v]$ denote the outputs of GT2-FLCs employing $P = a$ and $P = b$ α-planes, respectively. We also calculate the Average CTs (ACTs) over 10 experiments, by gridding the input space with 0.001 and 0.01 step sizes for GT2-SFLC and GT2-DFLC, respectively.

Simulations were performed on a computer with an Intel Core I7-9750H 2.6GHz processor, 8GB memory, running Windows10 64-bit and MATLAB R2019a. The CTs are obtained via *tic* and *toc* functions of MATLAB. During the experiments, the remaining DPs were set as follows:

- $\theta = -1$ and FOU-2 for the GT2-SFLC,
- $\theta = -1$ and FOU-3 for the GT2-DFLC.

Remark-2: In the experimental comparisons, we assume that the output of a continuous GT2-FLC (Y_c) can be approximated with a GT2-FLC employing $P = 1000$. Thus, we assume that $Y_C = Y_{1000}$ holds in our investigations.

We firstly compare the effect of P by comparing the outputs of GT2-FLCs with their continuous counterparts. The resulting mappings of GT2-SFLCs are shown in Fig. 6, while the ones for GT2-DFLCs are given in the Supplementary Material. The calculated measures are given in Tables IX and X for GT2-SFLCs and GT2-DFLCs, respectively.

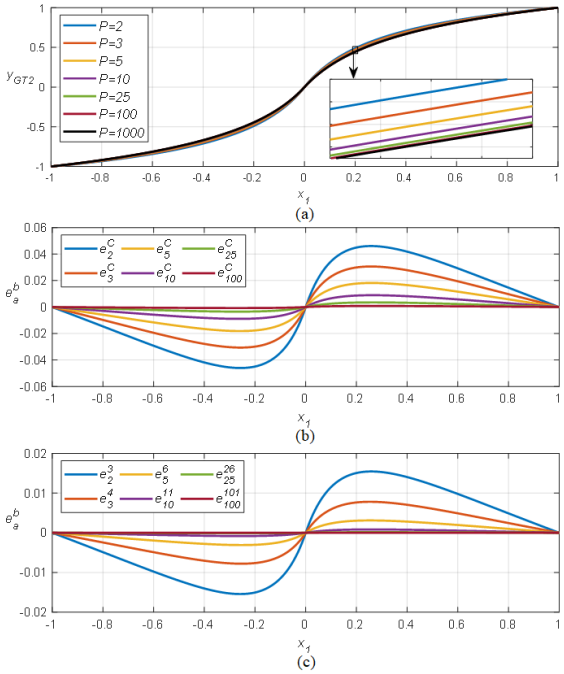

Fig. 6. Illustration of (a) the CCs for different P values, (b) the CC differences between Y_P and Y_C, and (c) the CC differences between Y_P and Y_{P+1}

It can be concluded that the mappings of the GT2-FLCs are almost identical as the P value varies through a wide range from 2 to 1000. This can also be numerically observed from Tables IX and X, as the GT2-FLCs resulted with relatively low MVE and MAE values, regardless of their P value. On the other hand, the P value has a significant effect on the ACT (as expected) and thus the deployment of a GT2-FLC employing high values of P might be an issue in real-time applications which usually require high sampling frequencies. For instance, when P was increased from 10 to 100 for the GT2-SFLC, the MVE measure was reduced from 8.925×10^{-3} to 0.798×10^{-3}, but the ACT value increased approximately 9 times. It is concluded that, more accurate CCs/CSs are generated with high values of P, which not too surprisingly increases the CT.

TABLE IX
SENSITIVITY MEASURES FOR GT2-SFLCS[1]

P	$MVE(e_P^C)$	$MAE(e_P^C)$	ACT (ms)	$MVE(e_P^{P+1})$	$MAE(e_P^{P+1})$
2	46.067	28.120	0.039±0.001	15.435	9.406
3	30.632	18.714	0.052±0.001	7.798	4.743
5	18.167	11.128	0.076±0.003	3.099	1.890
10	8.925	5.483	0.133±0.003	0.831	0.509
25	3.482	2.143	0.315±0.016	0.138	0.085
100	0.798	0.492	1.257±0.077	0.009	0.006

[1] The MAE and MVE values are normalized by 10^{-3}.

We also analyzed how the sensitivity of the CC/CS varies per increments of P (i.e. from P to $P + 1$). The results for SGFLCs are given in Fig. 6c while the ones for GT2-DFLCs are given in the Supplementary Material. The resulting MAE and MVE values are also given in Tables IX and X for GT2-SFLCs and GT2-DFLCs, respectively. For instance, increasing the P value from 3 to 4 resulted in a relatively bigger difference in terms of MAE and MVE when compared to the results in which P is increased from 100 to 101. It is concluded that the relative difference per increment decreases as P is getting bigger.

TABLE X
SENSITIVITY MEASURES FOR GT2-DFLCS[2]

P	$MVE(e_P^C)$	$MAE(e_P^C)$	ACT (ms)	$MVE(e_P^{P+1})$	$MAE(e_P^{P+1})$
2	48.577	23.783	0.133±0.012	16.295	7.975
3	32.281	15.814	0.147±0.014	8.342	4.022
5	19.140	9.393	0.169±0.014	3.299	1.598
10	9.407	4.625	0.224±0.015	0.878	0.430
25	3.701	1.808	0.356±0.017	0.146	0.072
100	0.860	0.415	1.017±0.051	0.010	0.005

[2] The MAE and MVE values are normalized by 10^{-3}.

B. Comments and Suggestions on the Sensitivity DP

The comparative analyses demonstrated that the sensitivity DP does not change the shape, but it determines the precision/ sensitivity of the CC/CS. The results also clearly show that there is a strong tradeoff between CT and CC/CS precision. In other words, high number of α-planes means accurate precision in the control signal, but huge computation burden at the same time. Thus, there is a need to provide a compromise in tuning the sensitivity of CC/CS, especially in real-time applications.

In real-time control applications, the designed GT2-FLCs are implemented on microcontroller-based hardware components which have a finite precision and processing power (i.e. CT). Moreover, GT2-FLCs have to not only process quantized input signals but also have to generate quantized output signals to be deployed to the real-world environment. In real-time applications, a continuous signal S is quantized as follows:

$$\hat{S} = \lfloor S/\Delta \rfloor \Delta \quad (41)$$

where $\hat{S}$ is the quantized signal, Δ is quantization level and $\lfloor\ \rfloor$ denotes the floor function. Thus, there is a quantization error

(Q_S) which is defined as follows:

$$Q_S = \hat{S} - S \tag{42}$$

The magnitude and characteristic of (42) will affect the real-time control performance of the GT2-FLC. Thus, Q_S has to be taken account in the design of GT2-FLCs.

We suggest one to tune the sensitivity DP P by taking into account the quantization level Δ and the required CT on the target hardware. In this context, we suggest designers to use the proposed iterative algorithm presented in the next subsection to provide a tradeoff between sensitivity and CT.

TABLE XI
TUNING ALGORITHM OF THE SENSITIVITY DP

Forward Calculation

Step 1: Define input and output quantization levels: Δ_{in} and Δ_{out}
Step 2: Quantize input values based on Δ_{in} according to (41)
Step 3: Calculate GT2-FLC output Y_2 via (16) with Δ_{in} for all inputs
Step 4: Obtain the quantized signal $\hat{Y}_2$ via (41) with Δ_{out}
Step 5: Define hyperparameters: $\varepsilon_1, P_f, P_{max}$
Step 6: Initialize $P_i = 0$, and $P^* = P_{max}$
Step 7: **for** $P = 3:1:P_{max}$ **do**
  Calculate GT2-FLC output Y_P via (16) with Δ_{in} for all inputs
  Obtain the quantized signal $\hat{Y}_P$ via (41) with Δ_{out}
  Calculate $MAE(e_P^{P-1})$ with $\hat{Y}_P$ and $\hat{Y}_{P-1}$ using (39)
  if $MAE(e_P^{P-1}) < \varepsilon_1$ **then**
    if $P_i == P_f$ **then**
      $P^* = P - P_f$
      break for loop
    end if
    $P_i = P_i + 1$
  else
    $P_i = 0$
  end if
end for
Output: The sensitivity DP $P = P^*$

Backward Calculation

Step 1: Take P^* and $\hat{Y}_{P^*}$ from the Forward Calculation
Step 2: Define hyperparameter: ε_2
Step 3: Initialize $P^{**} = 2$
Step 4: **for** $P = P^* - 1:-1:2$ **do**
  Calculate GT2-FLC output Y_P via (16) with Δ_{in} for all inputs
  Obtain the quantized signal $\hat{Y}_P$ via (41) with Δ_{out}
  Calculate $MVE(e_P^{P^*})$ with $\hat{Y}_P$ and $\hat{Y}_{P^*}$ using (38)
  if $MVE(e_P^{P^*}) > \varepsilon_2$ **then**
    $P^{**} = P + 1$
    break for loop
  end if
end for
Output: The sensitivity DP $P = P^{**}$.

C. Tuning Algorithm for the Sensitivity DP

Here, we present a novel iterative algorithm to tune the sensitivity DP (P) that accounts for hardware limits. The proposed algorithm is effective for real-time control problems, in which the CT and the sensitivity/quantization level (Δ) are fixed. The pseudo code is given in Table XI and has two steps:

1. **Forward calculation:** In this step, the goal is to find the GT2-FLC output under given sensitivity constraints and quantization levels of input/output signals. This is achieved by increasing the P value in each iteration to find a solution P^* such that the stopping condition is satisfied:

$$MAE(e_P^{P-1}) < \varepsilon_1 \tag{43}$$

where ε_1 is threshold value to be defined. However, because a floor operator is employed in the quantization, a chattering effect is usually observed; one must also check if the condition in (43) is also satisfied in interval of $[P^*, P^* + P_f]$ to conclude whether P^* is an acceptable solution. Here, $P_f > 0$ is a hyperparameter to be defined. This procedure can be viewed as an extra local search mechanism to handle the chattering phenomena in MAE. If the resulting ACT of the GT2-FLC is feasible for real-time application, there is no need for the next step.

2. **Backward calculation:** The calculated P^* in the forward calculation might result in a GT2-FLC that has high CT which may not be feasible for a real-time application. Therefore, in this step, we define an acceptable maximum precision error threshold (ε_2) to reduce the total number of α-planes which naturally reduces ACT (as shown in Section V.A). This is accomplished by decreasing P^* in each iteration until the MVE value, which is defined with respect to $\hat{Y}_{P^*}$,satisfies:

$$MVE(e_P^{P^*}) > \varepsilon_2 \tag{44}$$

In this way, a tradeoff between sensitivity and CT is obtained by finding a solution satisfying $P^{**} < P^*$. Note that, if there does not exist a solution which is feasible for the real-time application, then ε_2 is increased.

VI. REAL-TIME EXPERIMENTAL VALIDATION AND ANALYSIS

In this section, we present real-world experimental results using the Parrot Mambo drone, which is shown in Fig. 7, to evaluate the proposed design recommendations/methods for the design of GT2-FLCs. The Parrot Mambo drone has an ARM 9 416MHz processor and is equipped with 6-DOF IMU, pressure sensor, ultrasonic sensor, and a downward facing camera with a 60FPS. The drone has a MATLAB/Simulink support package to deploy control and sensor fusion algorithms. The drone has a highly efficient built-in flight control structure (from PI/PD controllers to Kalman estimators) to stabilize the attitude and altitude dynamics. The sampling time of flight algorithms of the Parrot Mambo is fixed as $T = 5ms$.

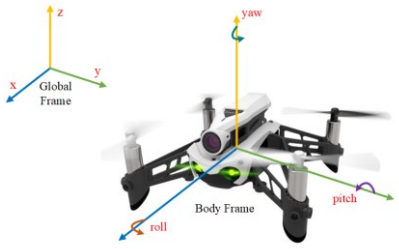

Fig. 7. Parrot Mambo drone with coordinate frames

In this study, we focused only on the design of the x-axis position controller that generates the pitch angle reference signal (u). During the design and experiments, the y-axis reference is set to 0m, the yaw angle reference is set to 0° and the altitude reference is set to 1m from the ground (controlled via built-in controllers). We preferred to design a PI type fuzzy controller that is formed using DFLC (i.e. T1, IT2 or GT2) with an integrator [3, 9]. The PI type DFLCs process the X-axis position error (e) and the change of X-axis position error (Δe)

to generate the pitch angle reference (u). The PI type DFLCs have two input scaling factors (K_e, $K_{\Delta e}$) and one output scaling factor (K_0) as given in the Supplementary Material. We handled the scaling factors as the main DPs of T1-DFLC since they affect the control performance [3, 5, 11-13].

A. Design of the Shape DP

In designing the shape DP (θ) of GT2-DFLC, we followed the steps given in Table VI. First, we designed baseline T1 and IT2 DFLCs for the steady state OP defined as $r = 1m$. The DPs of the baseline DFLCs are as follows:

- T1-DFLC: We designed a T1-DFLC with an aggressive CS, defined with the rule base given Table III, and set
$$K_e = 1, K_{\Delta e} = 0.68, K_0 = 2.5.$$
- IT2-DFLC: We designed an IT2-DFLC with a smooth CS and set
$$M_{1,1} = 0.05, M_{1,2} = 0.95, M_{1,3} = 0.05,$$
$$M_{2,1} = 0.15, M_{2,2} = 0.85\ , M_{2,3} = 0.15.$$

Then, the following GT2-DFLCs were designed:

- GT2-DFLC: We designed a GT2-DFLC with a fixed θ for the OP $r_1 = 1m$. The best θ value that provides a tradeoff was found experimentally as $\theta = 0.1$.
- GT2-DFLC with SM-1 (GT2-DFLC-SM-1): In the design of $f_r(r)$ in (35), we used the following steady state OPs $\boldsymbol{r} = [1m, 0.75m, 1.5m]$ and obtained $\boldsymbol{\theta_r} = [0.1, -0.8, 1]$ as the best values for these OPs. We used the linear interpolation method to define $f_r(r)$.
- GT2-DFLC with SM-2 (GT2-DFLC-SM-2): In the SM-2 design, the $f_r(r)$ designed for GT2-DFLC-SM-1 was used. The design of $f_t(x)$ in (37) was accomplished via the rule-base given in Table VIII with $w = 0.5$.

The CSs of all DFLCs and their CS comparisons are given in Section S.3 which is presented in the Supplementary Material.

B. Design of the Sensitivity DP

In designing the sensitivity DP (P) of the GT2-DFLC, we took into account the hardware limitations of the real-world drone, which are Δ and CT. Because the Parrot Mambo drone is equipped with various sensors with different resolutions, we assumed that the average quantization levels are approximately $\Delta_{in} = 0.01$ and $\Delta_{out} = 0.001$. To study whether the CT of designed GT2-FLCs are then feasible for a real-time flight, we examined the CT of the built-in flight control system via the MATLAB Simulink Profiler toolbox to find a maximum allowable CT for GT2-DFLC. The ACT of flight control system is found as $T_{FC} \approx 3.7ms$, and thus there is $T - T_{FC} \approx 1.3ms$ left for the computations of the GT2-DFLC.

To tune the sensitivity DP of the designed GT2-DFLC, we employed the iterative algorithm given in Table XI. The forward calculation step stopped at $P^* = 23$ for the settings $\varepsilon_1 = 0.025 \times 10^{-3}$, $P_f = 20$, and $P_{max} = 100$. In order to conclude whether the resulting $P^* = 23$ is feasible for the real-time application, we calculated the ACT of the GT2-DFLC with $P = 23$ on the computer and obtained approximately 0.348ms. Then, we multiplied this value by 6.25 and obtained $T_{GT2} = 2.176ms$ (since the clock speed ratio between the processors of the computer and the Parrot Mambo is 6.25). To cope with resulting errors of this rough ACT mapping from a 2.6GHz to 416MHz processor, we left a buffer time value of at least 0.3ms and observed that the GT2-DFLC with $P^* = 23$ is not feasible since the total CT ($T_{FC} + T_{GT2} + 0.3$) is higher than the sampling time of the drone ($T = 5ms$). To overcome this problem, the backward calculation step in Table XI was performed with $\varepsilon_2 = 0.01$ and P^{**} was obtained as 4. The ACT of GT2-DFLC employing $P = 4$ α-planes was examined and then it was found that $T_{GT2} = 0.978ms$. We concluded that the ACT of the designed GT2-DFLC employing $P = 4$ α-planes is feasible for real-time applications on the Parrot Mambo drone.

Remark-3: As we just stated, we mapped the ACTs of the GT2-DFLC by multiplying the results calculated from a computer with 6.25 since the Parrot Mambo drone has a 416MHz processor which is approximately 6.25 times slower than the clock speed of the processor of the computer (2.6GHz). Although clock speed is an important indicator of how fast the processor is, it is not the only factor, since different processors often use different architectures, and other factors (e.g. cache size, speed of RAM) also contribute to the overall performance of the processor. For this reason, we defined a buffer time value of at least 0.3ms.

C. Experimental Results

The performances of the DFLCs were compared with respect to overshoot (*OS%*), rise time (T_r) and settling time for 5% tolerance band (T_s) values. The performance of DFLCs for the OPs ($\boldsymbol{r} = [1m, 0.75m, 1.5m]$) are given in Fig. 8 and Fig. 9, while the performance measures are given in Table XII.

The performance of the GT2-DFLC with $\theta = 0.1$ is compared with its T1 and IT2 counterparts as given in Fig. 8. Observe:

- From Fig. 8 and Table XII that the lowest OS% values are calculated for the IT2-DFLC as it has been designed with a smooth CS, while the lowest T_r value is obtained for the T1-DFLC as it has been designed with an aggressive CS. As shown in Figs. S11-S12 (given in the Supplementary Material), the CS of GT2-FLC is smoother than its T1 while more aggressive than its IT2 baselines. As an outcome of this shape DP design, for the first OP change, the GT2-DFLC improves the T_r value by 0.27s by compromising the OS% value by 5.83% in comparison to its IT2 baseline, while it improves the OS% value of T1-FLC by almost 3% by compromising 0.06s for the T_r. The performance of the GT2-DFLC lies between its T1 and IT2 DFLCs and thus provides a compromise between its baseline DFLCs.
- From Fig. 8b that, since the performance of the baseline T1 and IT2 DFLCs degraded at this OP, the performance of GT2-DFLC degraded in comparison to the results given in Fig. 8a. This is due to the fact that the GT2-DFLC literally schedules the outputs of its baseline T1 and IT2 DFLCs, so its performance heavily depends on its baseline DFLCs.

The performances of the GT2-DFLCs with SMs are compared with the GT2-DFLC with $\theta = 0.1$ in Fig. 9. Observe:

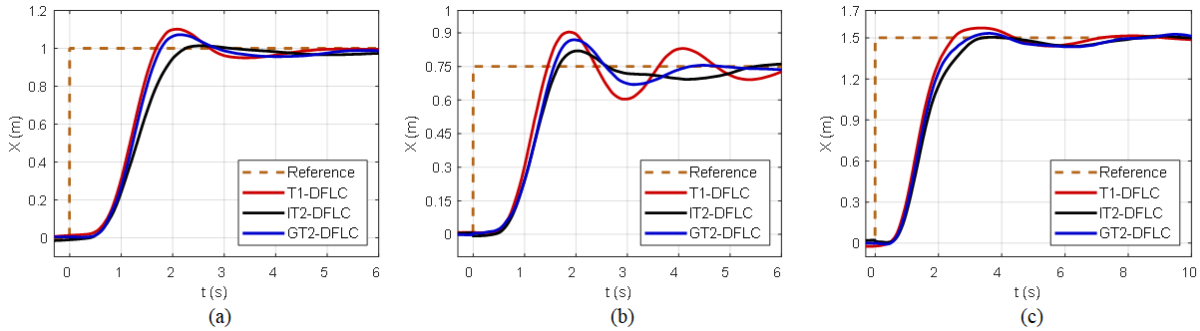

Fig. 8. Illustration of the performances of the T1, IT2 and GT2 DFLCs for (a) $r_1 = 1m$ (b) $r_2 = 0.75m$ (c) $r_3 = 1.5m$

TABLE XII
PERFORMANCE MEASURES OF THE REAL-TIME CONTROL EXPERIMENTS

Controller	OP-1			OP-2			OP-3		
	T_s (s)	OS%	T_r (s)	T_s (s)	OS%	T_r (s)	T_s (s)	OS%	T_r (s)
T1-DFLC	3.54	10.13	0.79	5.85	20.47	0.65	2.25	4.80	1.23
IT2-DFLC	2.01	1.39	1.12	4.86	9.28	0.79	2.84	0.92	1.64
GT2-DFLC	2.44	7.22	0.85	3.75	15.87	0.75	2.54	2.20	1.39
GT2-DFLC-SM-1	2.44	7.22	0.85	5.78	9.39	0.69	2.16	4.84	1.18
GT2-DFLC-SM-2	1.79	3.39	0.88	4.05	6.64	0.74	2.16	2.91	1.15

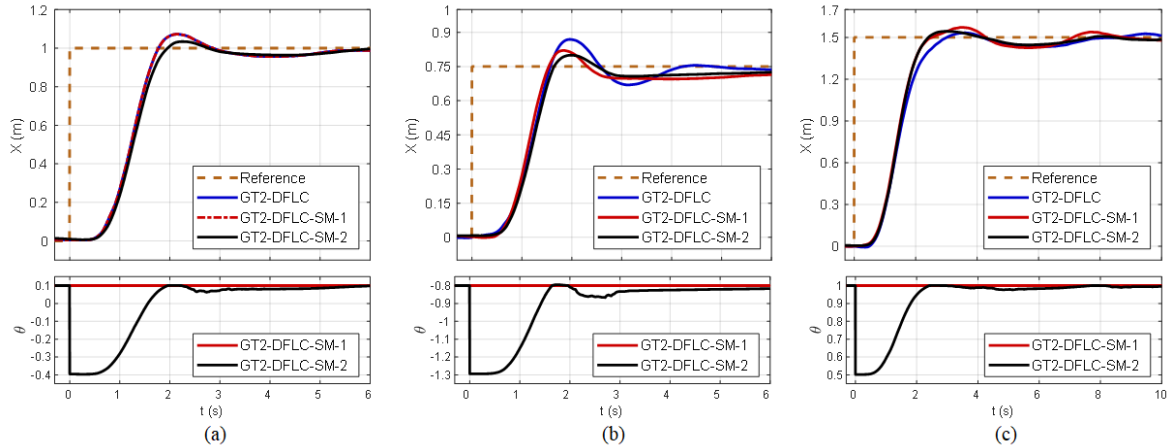

Fig. 9. Illustration of the performances of the GT2-DFLC, GT2-DFLC-SM-1 and GT2-DFLC-SM-2 for (a) $r_1 = 1m$ (b) $r_2 = 0.75m$ (c) $r_3 = 1.5m$

- From Fig. 9 that updating the shape DP with respect to the OP results in a highly efficient control system response both in the sense of control performance and robustness.
- From Fig. 9b that the SM-2 reduced θ to -1.3 (i.e. the aggressiveness of the CS is reduced) and then dynamically increased θ to its nominal value of -0.8. This results in a performance without oscillation and less overshoot. As given in Table XII, the GT2-DFLC-SM-2 reduced the OS% and *Ts* values by 2.64% and 0.81s respectively, since the SM-2 transformed its mapping into a CS which is smoother than its IT2 fuzzy counterpart as shown in the Fig. S17b (presented in the Supplementary Material).
- From Fig. 9c that theSM-2 changed θ from 0.5 to 1, and thus increased dynamically the aggressiveness of the CS to end up with faster transient system response in comparison to the GT2-DFLC with fixed of $\theta = 0.1$, which resulted in a relatively slow system response.
- That both SM-1 and SM-2 enhanced the control system performance but the SM-2, which takes into account the transient state dynamics and OP to tune the shape DP, resulted in superior control performances for all OPs.

We conclude that the online tuning of the shape DP with respect to the OP has the potential to provide a good tradeoff between robustness and performance via the proposed SM-1 and SM-2.

VII. CONCLUSIONS AND FUTURE WORK

We have provided a new perception of how GT2-FSs affect the CC/CS of GT2-FLCs and have also presented a systematic design approach for GT2-FLCs. To ease the design of GT2-FLCs, we first provided general suggestions on the structural settings and then defined their main DPs. We suggested employing trapezoid SMFs as they provide a great design flexibility. We also proposed a mapping for trapezoid SMF that provides the opportunity to transform the trapezoid SMF into a crisp, interval, triangular SMF via a single tuning parameter.

We addressed the challenge of GT2-FSs that are usefulness and interpretation of the SMFs by providing the DPs with interpretations about the sensitivity and shape of the CC/CS. We first presented analyses to provide explanations about the role of the shape DP on CC/CS. We concluded that the shape DP provides not only design simplicity as only baseline T1 and IT2 FLCs are needed, but also a convenient design flexibility as a tradeoff between performance (i.e. like a T1-FLC) and robustness (i.e. like an IT2-FLC) can be easily provided. Then,

to enhance the control performance, we proposed SMs that tune the shape DP in an online manner with respect to the OP. This results with a GT2-FLC that basically uses and schedules a collection of T1 and IT2 FLCs to end up with a satisfactory performance. Then, we provided practical insights into how to tune the sensitivity DP by showing how the sensitivity of the CC/CS and CT is affected. We presented an algorithm for tuning the sensitivity DP by providing a tradeoff between sensitivity and CT which are essential factors to be taken account in real-time applications. We also designed GT2-FLCs to control a real-world drone and validated our proposed design approaches with proof of concept real-time experiments.

We believe that the results of this study will open the doors to a wider use of GT2-FLCs in real-time applications as we provided interpretations to the DPs and proposed design approaches by taking account the resulting effect of the DPs on the GT2-FLC's performance, robustness, sensitivity and CT.

As for our future work, we plan to extend the presented analysis and design methodologies by 1) investigating other type of SMFs (like Gaussian) towards more generic definitions, 2) deriving the analytical relationship of the GT2-FLC and providing an interpretation, 3) developing sophisticated tuning mechanisms for the shape and sensitivity DP, 4) employing neural networks and optimizations algorithms to tune GT2-FLCs, and 5) examining the performance of the proposed GT2-FLCs in challenging real-world experiments.

ACKNOWLEDGMENT

The authors would like to thank the editor and reviewers of this paper for their very insightful and constructive comments.

REFERENCES

[1] J. M. Mendel, *Uncertain Rule-Based Fuzzy Systems, Introduction and New Directions, Second Ed.*, Springer, Cham, Switzerland, 2017.

[2] J. M. Mendel, H. Hagras, W. W. Tan, W. W. Melek, and H. Ying, *Introduction to Type-2 Fuzzy Logic Control*, John Wiley and IEEE Press, Hoboken, NJ, 2014.

[3] R. K. Mudi and N. R. Pal, "A robust self-tuning scheme for PI- and PD type fuzzy controllers," *IEEE Trans. Fuzzy Systems*, vol. 7, no. 1, pp. 2-16, February 1999.

[4] P. Korba, R. Babuska, H. B. Verbruggen, and P. M. Frank, "Fuzzy Gain scheduling: controller and observer design based on Lyapunov method and convex optimization," *IEEE Trans. Fuzzy Systems*, vol. 11, no. 3, pp. 285-298, June 2003.

[5] X. G. Duan, H. X. Li, and H. Deng, "Effective tuning method for fuzzy PID with internal model control," *Ind. Eng. Chem. Res.*, vol. 47, pp. 8317-8323, October 2008.

[6] H. A. Hagras, "A hierarchical type-2 fuzzy logic control architecture for autonomous mobile robots," *IEEE Trans. Fuzzy Systems*, vol. 12, no. 4, pp. 524–539, August 2004.

[7] D. Wu and W. W. Tan, "Genetic learning and performance evaluation of interval type-2 fuzzy logic controllers," *Engineering Applications of Artificial Intelligence*, vol. 19, no.8, pp. 829-841, December 2006.

[8] M. Biglarbegian, W. W. Melek, and J. M. Mendel, "On the stability of interval type-2 TSK fuzzy logic control systems," *IEEE Trans. Systems, Man, Cybernetics B, Cybernetics*, vol. 40, no. 3, pp. 798–818, June 2010.

[9] X. Du and H. Ying, "Derivation and analysis of the analytical structures of the interval type-2 fuzzy-PI and PD controllers," *IEEE Trans. Fuzzy Syst.*, vol. 18, no. 4, pp. 802–814, August 2010.

[10] D. Wu, "On the fundamental differences between interval type-2 and type-1 fuzzy logic controllers," IEEE *Trans. Fuzzy Systems,* vol. 20, no. 5, pp. 832-848, October 2012.

[11] A. Sakalli, T. Kumbasar, E. Yesil, and H. Hagras "Analysis of the performances of type-1, self-tuning type-1 and interval type-2 fuzzy PID controllers on the magnetic levitation system," *in Proc. of IEEE Int. Conf. on Fuzzy Systems*, July 2014.

[12] T. Kumbasar, "Robust stability analysis and systematic design of single-input interval type-2 fuzzy logic controllers," IEEE *Trans. Fuzzy Systems,* vol. 24, no. 3, pp. 675-694, June 2016.

[13] E. Yesil, "Interval type-2 fuzzy PID load frequency controller using big bang–big crunch optimization," *Applied Soft Computing*, vol. 15, pp. 100–112, February 2014.

[14] H. Bustince, J. Fernandez, H. Hagras, F. Herrera, M. Pagola, and E. Barrenechea, "Interval type-2 fuzzy sets are generalization of interval-valued fuzzy sets: towards a wide view on their relationship," *IEEE Trans. Fuzzy Systems*, vol. 23, pp. 1876–1882, October 2015.

[15] A. Sarabakha, C. Fu, and E. Kayacan, "Intuit before tuning: type-1 and type-2 fuzzy logic controllers," *Applied Soft Computing,* vol. 81, August 2019.

[16] A. Sakalli, A. Beke, and T. Kumbasar, "Gradient descent and extended Kalman filter based self-tuning interval type-2 fuzzy PID controllers," *in Proc. of IEEE Int. Conf. on Fuzzy Systems*, July 2016.

[17] A. Sakalli, A. Beke, and T. Kumbasar, "Analyzing the control surfaces of type-1 and interval type-2 FLCs through an experimental study," *in Proc. of IEEE Int. Conf. on Fuzzy Systems*, July 2018.

[18] A. Sakalli, T. Kumbasar, F. Dodurka, and E. Yesil, "The simplest interval type-2 fuzzy PID controller: Structural analysis," *in Proc. of IEEE Int. Conf. on Fuzzy Systems*, July 2014.

[19] A. Sakalli and T. Kumbasar, "On the design and gain analysis of IT2-FLC with a case study on an electric vehicle," *in Proc. of IEEE Int. Conf. on Fuzzy Systems*, July 2017.

[20] A. Sakalli and T. Kumbasar, "On the fundamental differences between the NT and the KM center of sets calculation methods on the IT2-FLC performance," *in Proc. of IEEE Int. Conf. on Fuzzy Systems*, August 2015.

[21] C. Wagner and H. Hagras, "Toward general type-2 fuzzy logic systems based on zSlices," *IEEE Trans. Fuzzy Systems,* vol. 18, no. 4, pp. 637-660, August 2010.

[22] T. Kumbasar and H. Hagras "A self-tuning zSlices based general type-2 fuzzy PI controller," *IEEE Trans. Fuzzy Systems,* vol. 23, no. 4, pp. 991-1013, August 2015.

[23] M. A. Sanchez, O. Castillo and J. R. Castro, "Generalized type-2 fuzzy systems for controlling a mobile robot and a performance comparison with interval type-2 and type-1 fuzzy systems," *Expert Systems with Applications*, vol. 42, no. 14 pp. 5904-5914, August 2015.

[24] O. Castillo, L. A.-Angulo, J. R. Castro and M. G.-Valdez, "A comparative study of type-1 fuzzy logic systems, interval type-2 fuzzy logic systems and generalized type-2 fuzzy logic systems in control problems," *Information Sciences*, vol. 354, pp. 257-274, August 2016.

[25] A. Mohammadzadeh, S. Ghaemia, O. Kaynak and S. Khanmohammadi, "Observer-based method for synchronization of uncertain fractional order chaotic systems by the use of a general type-2 fuzzy system," *Applied Soft Computing,* vol. 49, pp. 554-560, December 2016.

[26] M. H. Khoobana, N. Vafamand, A. Liaghat and T. Dragicevic, "An optimal general type-2 fuzzy controller for urban traffic network," *ISA Transactions,* vol. 66, pp. 335-343, January 2017.

[27] O. Castillo and L. A.-Angulo, "A generalized type-2 fuzzy logic approach for dynamic parameter adaptation in bee colony optimization applied to fuzzy controller design," *Information Sciences*, vol.460-461, pp. 476-496, September 2018.

[28] J. M. Mendel, "Comparing the performance potentials of interval and general type-2 rule-based fuzzy systems in terms of sculpting the state space," *IEEE Trans. on Fuzzy Systems*, vol. 27, no. 1, pp. 58-71, January 2019.

[29] J. M. Mendel, "Explaining the performance potential of rule-based fuzzy systems as a greater sculpting of the state space," *IEEE Trans. on Fuzzy Systems,* vol. 26, no. 4, pp. 2362-2373, August 2018.

[30] J. Z. Shi, "A fractional order general type-2 fuzzy PID controller design algorithm," *IEEE Access*, vol. 8, 52151-52172, March 2020.

[31] J. M. Mendel, F. Liu and D. Zhai, "α-plane representation for type-2 fuzzy sets: Theory and applications," IEEE *Trans. Fuzzy Systems,* vol. 17, no. 5, pp. 1189-1207, October 2009.

[32] J. M. Mendel, "Comments on 'α-plane representation for type-2 fuzzy sets: theory and applications'," *IEEE Trans. on Fuzzy Systems*, vol. 18, no.1, pp. 229-230, February 2010.

[33] D. Zhai and J. M. Mendel, "Comment on "toward general type-2 Fuzzy logic systems based on zSlices"," *IEEE Trans. Fuzzy Systems*, vol. 20, no. 5, pp. 996–997, October 2012.

[34] V. Vesely, A. Ilka, "Gain-scheduled PID controller design," *Journal of Process Control,* vol. 23, no. 8, pp. 1141-1148, September 2013.

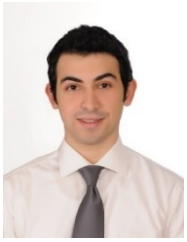

AHMET SAKALLI (S'13) received the B.Sc. and M.Sc. degrees in control and automation engineering from Istanbul Technical University, in 2012 and 2014, respectively. He is currently pursuing the Ph.D. degree with the Control and Automation Engineering Department, Faculty of Electrical and Electronics Engineering, Istanbul Technical University. He is working as a lead systems engineer at AVL Research and Engineering Turkey. His research interests are in computational intelligence, type-2 fuzzy logic, fuzzy control, evolutionary algorithms, and control theory as well as their real-world applications.

TUFAN KUMBASAR (M'13-SM'19) received the B.Sc. and M.Sc. and Ph.D. degrees in control and automation engineering from the Istanbul Technical University. He is currently an Associate Professor in the Control and Automation Engineering Department and the director of Artificial Intelligence and Intelligent Systems (AI^{2}S) Laboratory, Faculty of Electrical and Electronics Engineering, Istanbul Technical University.

He has currently authored more than 100 papers in international conferences, journals, and books. His major research interests are in computational intelligence, notably type-2 fuzzy logic, fuzzy control, neural networks, evolutionary algorithms, and control theory. He is also interested in robotics, machine learning, intelligent control, and their real-world applications. He has served as a Publication Co-Chair, Panel Session Co-Chair, Special Session Co-Chair, PC, IPC, and TPC in various international and national conferences. Dr. Kumbasar is an Associate Editor for the IEEE TRANSACTIONS ON FUZZY SYSTEMS and an Area Editor for the INTERNATIONAL JOURNAL OF APPROXIMATE REASONING.

Dr. Kumbasar received the Best Paper Awards from the *IEEE International Conference on Fuzzy Systems* in 2015, and from the *6th International Conference on Control Engineering & Information Technology* in 2018.

JERRY M. MENDEL (LF'04) received the Ph.D. degree in electrical engineering from the Polytechnic Institute of Brooklyn, Brooklyn, NY. Currently, he is Emeritus Professor of Electrical Engineering at the University of Southern California in Los Angeles.

He has published over 580 technical papers and is author and/or co-author of 13 books. He is a Life Fellow of the IEEE, a Distinguished Member of the IEEE Control Systems Society, and a Fellow of the International Fuzzy Systems Association. He was a member of the Administrative Committee of the IEEE Computational Intelligence Society for nine years, and Chairman of its Fuzzy Systems Technical Committee and the Computing With Words Task Force of that TC. Among his awards are four IEEE Transactions Best/Outstanding paper awards, a 1984 IEEE Centennial Medal, an IEEE Third Millennium Medal, and a Fuzzy Systems Pioneer Award (2008) from the IEEE Computational Intelligence Society. His present research interests include: type-2 fuzzy logic systems and computing with words. He has more than 54,000 citations to his publications on Google Scholar.